Hindawi
International Journal of Polymer Science
Volume 2021, Article ID 4954837, 11 pages
https://doi.org/10.1155/2021/4954837

*Research Article*

# The Study of Bound Water Status and Pore Size Distribution of Chinese Fir and Poplar Cell Wall by Low-Field NMR

**Huimin Cao, Jianxiong Lyu, Yongdong Zhou, and Xin Gao**

*Research Institute of Wood Industry, Chinese Academy of Forestry, Dongxiaofu No. 1, Xiangshan Road, Beijing 100091, China*

Correspondence should be addressed to Xin Gao; gaoxin@caf.ac.cn

Received 31 May 2021; Accepted 10 August 2021; Published 26 August 2021

Academic Editor: Yun Lu



With the increasing shortage of timber resources and the advancement of environmental protection projects, many artificial fast-growing forests are planted and used as raw materials in China. There are significant differences in the properties of natural forest wood and artificial fast-growing forest wood, and the properties of wood mainly depend on the change in the status of bound water in the cell wall. In this study, the fiber saturation point (FSP) and pore size distributions within the cell wall of six species of fast-growing forest wood were studied by low-temperature nuclear magnetic resonance (NMR) technology. The effects of species, growth rings, and extractives on the FSP and pore structure were analyzed. The water vapor sorption experiments were performed, and the adsorption isotherms of the samples were fitted through the Guggenheim-Anderson-de Boer (GAB) equation. According to the least-square regression of the adsorption isotherms and combined with the low-temperature NMR experiments, the content and proportion of the different types of bound water were analyzed. The results showed that the average FSP of each Chinese fir was about 40% and that of each poplar was about 35%. There is about a 10% difference between the FSP measured by NMR technology and the adsorption bound water content obtained by adsorption isothermal. The pore size distribution results show that in all samples, the proportion of pores larger than 10.5 nm is very low, about 10%; the proportion of 1.92-10.5 nm pores is about 30%; and the proportion of pores smaller than 1.92nm is more than 50%. This work will be helpful to the study of the wood moisture status and provide reference data for wood modification.

## 1. Introduction

Wood is a versatile renewable engineering material that has been widely used in construction and decoration. This can be attributed to its superior material properties, such as a favorable mass strength ratio, easy processing, and environmental characteristics [1, 2]. As a major country in the production and processing of wood products, China has consumed approximately 600 million cubic meters of wood annually in recent years [3]. With the increasing shortage of timber resources and the advancement of environmental protection projects, many artificial fast-growing forests are used as raw materials in the wood industry. Chinese fir and poplar are the two most planted artificial fast-growing forest species, and their plantation area ranks among the top in China [4]. With the advantages of a fast growth rate, Chinese fir and poplar have been widely used in furniture, construction, wood-based panel, and other products. However, due to the fast growth rate, the dimensional stability, density, strength, durability, and other properties of fast-growing forest wood are not as good as natural forest wood [5].

As a special kind of biomass porous material, wood continually exchanges moisture with the surroundings [6]. It is generally accepted that moisture in wood exists in two basic forms, bound water within the cell wall and free water in lumens, such as the vessel, fiber, tracheid, and ray. The concept of the fiber saturation point (FSP) is introduced into the study of wood moisture status, which is defined as the moisture content at which the cell wall is saturated with bound water with no free water in the lumens [7]. Below FSP, as the bound water content changes, the wood dimensions, mechanical strength, electrical conductivity, and other properties of wood change significantly accordingly [8]. Above the FSP, the properties of wood do not change significantly with moisture content. Therefore, the fiber saturation point

is recognized as the transition point of wood properties. Several methods have been used to measure FSP, such as extrapolation methods (by extrapolating adsorption isotherms or physical property changes with moisture content), solute exclusion, porous plate, centrifugal dehydration, differential scanning calorimetry (DSC), and nuclear magnetic resonance (NMR) [9–16]. It is considered that the value of FSP could be strongly influenced by the method used, and the values of FSP obtained by different methods varied in the range of 13% to 70% [17]. The value of FSP determined by extrapolation methods is usually approximately 30%. However, the FSP determined by extrapolation methods may underestimate the saturated content of bound water. Methods including solute exclusion, porous plate, DSC, and NMR may result in FSP values above 40% [18].

The pore structure of wood, especially the pore size distribution within the cell wall, is also an important parameter. As mentioned earlier, the dimensional stability, strength, and durability of fast-growing wood in plantations often need to be enhanced. Water soluble polymers such as urea resin, phenolic resin, and functional nanoparticles, such as copper carbonate and iron oxide, have been used to improve the properties of wood by vacuum-pressure impregnation. It has been widely agreed that only the deposition of polymer within the cell wall results in improvement of the dimensional stability as well as a high decay resistance [19]. There are a few methods used to determine the pore size distribution of porous materials, including mercury intrusion method, gas adsorption ($N_2$ or $CO_2$), scanning electron microscope (SEM), and atomic force microscope (AFM) [20–23]. However, these methods are restricted when applied to measuring the pore size distribution of the wood cell wall. First, these methods are generally destructive and invasive; there is a significant influence on the testing results when they are applied to relatively soft wood material. Second, there is adsorbed water in the porous medium because of the hygroscopic substrate and capillary condensation effect. The test specimen should be dried prior to the experiment. The pore structure of the wood cell wall would significantly change during the drying process. The cell wall of timber after vacuum-pressure impregnation is saturated with water-soluble modifying agents, it is necessary to know the pore size distribution within the cell wall corresponding to this state [24].

NMR cryoporometry is a technique for nondestructively determining pore size distributions in the porous medium through the observation of the depressed melting point of a confined liquid; therefore, it is also one of the few methods that can determine the pore size distributions of the porous medium containing moisture or other liquids. The applications of NMR cryoporometry include studies of silica gels, bones, cement, rocks, and many other porous materials. The pore size distributions of wood and heat-treated wood have also been analyzed [25–27].

In addition to the analysis of the wood pore structure, NMR has also been widely used in other related research fields of wood physics and chemistry. The structure of natural and modified wood has been investigated by 1H, 13C spectrum, cross-polarization magic angle spinning (CP-MAS), and other NMR techniques [28]. In recent years, low-cost NMR equipment with magnetic field strength has also been used in wood-water relations, such as $T_1$ and $T_2$ relaxation time distributions [29]. As the relaxation signal amplitude of moisture in wood is directly proportional to the mass of moisture, the moisture content can be quantitatively determined by NMR signals [30]. Portable NMR devices are also used as nondestructive tools for moisture content measurement [31]. The relaxation distributions can provide more detailed information about the states of moisture in wood. The bound water within the cell wall and free water in the lumens can be qualitatively analyzed according to the $T_2$ relaxation time distributions [32]. The FSP of green wood and heat-treated wood has been determined by comparing the signal amplitude of moisture in wood samples above and below the melting point water. At the same time, the freezing bound water and nonfreezing bound water in the cell wall can also be determined [27]. 2D ($T_1$-$T_2$, $T_2$-$D$) NMR, Fast Field Cycling NMR (FFC-NMR), magnetic resonance imaging (MRI), and other NMR techniques have also been employed to study the wood-water relations and moisture transfer in wood [33, 34].

In this work, the FSP and pore size distributions within the cell wall of six species of fast-growing forest wood were studied by low-temperature NMR technology. The effects of species, growth rings, and extractives on the FSP and pore structure were analyzed. After the NMR experiment, the water vapor sorption experiments were performed in the two-chamber setup, and the adsorption isotherms of the samples were fitted through the GAB equation. The monolayer molecular water content, multilayer molecular water content, and theoretical limit content of bound water (determined by the extrapolation method) were obtained by least-square regression of adsorption isotherms. Combined with the actual value of the FSP determined by the NMR method, the content of different types bound water was analyzed. This work will be helpful to the study of the wood moisture status and provide reference data for wood modification.

## 2. Materials and Methods

*2.1. Materials.* Three species of clonal Chinese fir (*C. lanceolata*) and three species of clonal poplar (*Populus deltoides*) were used as the materials; they were all artificial fast-growing wood and widely planted in China. The basic information of the experimental materials is shown in Table 1. Trees were harvested by sawing at breast height to obtain discs with a thickness of approximately 20 mm, sealed in bags, and stored at -4°C. The discs were removed from the cold storage before the NMR experiments, sliced to a width of 20 mm, and passed through a strip of medullary wood. Then, the specimens were processed to dimensions of 20 mm × 8 mm × 8 mm (longitudinal × radial × radial, $L \times T \times R$) in a growth ring. F24×Na 1-1 and Kaihua 13 contained approximately 20 to 21 growth rings; however, after the 14th growth ring, the growth rate of these fir species slowed, and the last 10 mm width near the bark contained six to seven growth rings. Because of the requirement of signal quantity and signal-to-noise ratio in nuclear NMR, the

Table 1: Sample information.

| Species | Sampling site | Longitude and latitude | Average diameter at breast height (cm) | Average tree height (m) | Afforestation time | Sampling time |
|---|---|---|---|---|---|---|
| F24×Na 1-1 | Kaihua, Zhejiang | 118°01′E, 28°54′N | 24.7 | 22.9 | 1998 | 2017 |
| Kaihua 13 | Kaihua, Zhejiang | 118°01′E, 28°54′N | 18.4 | 16.8 | 1998 | 2017 |
| Yang 020 | Nanping, Fujian | 118°08′E, 27°38′N | 16.2 | 17.5 | 2008 | 2018 |
| 55/65 | Jiaozuo, Henan | 113°27'E,35°13'N | 22.6 | 19.5 | 2009 | 2017 |
| Nanyang | Jiaozuo, Henan | 113°27'E,35°13'N | 20.2 | 17.6 | 2009 | 2017 |
| Zhongliao 1 | Huludao, Liaoning | 120°38'E,40°56'N | 24.2 | 16.4 | 2010 | 2018 |

extremely narrow growth ring cannot be separated independently. Therefore, F24×Na 1-1 and Kaihua 13 were determined to have one to 14 independent growth rings and 15 (containing multiple growth rings) in a total of 15 samples. Yang 020 was separated into nine independent growth rings and 10 (containing multiple growth rings) in a total of 10 samples. There were no narrow growth rings in the asexual line of plantation poplar. 55/65 and Nanyang had independent growth rings from one to 10, and Zhongliao 1 had independent growth rings from one to nine.

*2.2. Equipment.* The low-temperature NMR experiments were performed on a 23 MHz mini-NMR instrument (NMRC12-010V, Niumag Instruments, Suzhou, China), and the sample chamber contained a temperature-controlling system ranging from -45°C to 50°C with an accuracy of 0.1°C. A vacuum-pressure saturation device (Jiangsu Huaxing Scientific Instruments Company, Nantong, China) was used to saturate the sample with water. The size of the sample chamber is $\varphi$120 mm × 400 mm. The maximum vacuum is $7 \times 10^{-6}$ Pa, and the pressure limit is 50 MPa.

*2.3. Sample Treatment.* The 3-4 cm thickness discs at the breast height (approximately 1.5 m) were cut from each tree and were kept in closed, plastic bags in a freezer until sample preparation. Before the experiments, strips of wood passing through the center were cut from the discs. To make the cell wall of the wood strips fully saturated with water, the strips were treated through a vacuum-pressure process, maximum vacuum for 30min, and then 1.5 MPa for 120 min. Cuboid sample pieces (approximately 8 mm × 8 mm × 20 mm, 20 mm in the longitudinal direction) were cut from each growth ring using a microtome blade. However, when the age of the Chinese fir exceeds a certain number of years, its growth rate slows down and the growth ring width becomes narrower. In order to ensure the signal-to-noise ratio during the NMR experiments, the sample size must maintain certain requirements. The last sample near the sapwood may contain multiple growth rings.

*2.4. NMR Experiments.* The samples were placed in 10 mm OD NMR tubes closed with Teflon caps and then were sealed with laboratory film (Parafilm 996) during experiments. The sample was then frozen, and the $T_2$ scanning at different temperatures was performed beginning with the lowest temperature (from -45°C to 20°C). To ensure that the sample reaches the set temperature, a fiber optic temperature sensor is placed in the sample tube. When the temperature sensor reaches the set temperature, we continue to maintain the temperature for 30 min to ensure that the sample's temperature is uniform.

The mass change of the samples before and after NMR scanning was no more than 1%. Therefore, it was considered that the sample tube had a good seal, and the mass change during the NMR experiment could be ignored. The $T_2$ relaxation times of the samples were obtained using the CPMG sequence [15].

$$90\circ_x - \tau - \left[180\circ_y - \tau - \text{echo} - \tau\right]_n - \text{rt}, \quad (1)$$

Table 2: The relationship between the temperature drops of the freezing point and pore diameter.

| $T_m(D)$ (°C) | $D$ (nm) |
|---|---|
| -30°C | 1.92 |
| -25°C | 2.18 |
| -20°C | 2.58 |
| -15°C | 3.24 |
| -10°C | 4.56 |
| -5°C | 8.52 |
| -4°C | 10.5 |
| -3°C | 13.8 |
| -2°C | 20.4 |
| -1°C | 40.2 |

where $\tau$ is the time delay, and $\tau = 0.1$ ms. $n$ is the total number of echoes, and $n = 15{,}000$. The recycle time (rt) and the number of accumulated scans were 1 s and 64, respectively. The echo time in the sequence was 0.1 ms, the macromolecule and frozen water (ice) with $T_2 < 0.1$ ms were not detectable in these $T_2$ measurements.

The basis to measure the pore size distribution using NMR cryoporometry is the observation of the depressed melting point of a confined liquid; the relationship between the pore diameter and the melting point depression was described by the Gibbs-Thomson equation:

$$\Delta T_m = T_m - T_m(D) = \frac{4\sigma T_m \cos\theta}{D\Delta H_f \rho}, \quad (2)$$

where $T_m$ is the freezing point of macroscopic water, $T_m(D)$ is the freezing point of pore water with $d$ diameter, $\Delta T_m$ is the difference between the freezing point of pore water and macroscopic water, $\sigma$ is the free energy, $\rho$ is the density of water, $H_f$ is the specific enthalpy, and $\theta$ is the contact angle. The above values were set to $T_m = 273.15$ k, $\sigma = 12.1$ mJ m$^{-2}$, $\theta = 180°$, $\rho = 1.0 \times 10^3$ kg m$^{-3}$, $H_f = 333.6$ J g$^{-1}$ [35]. The corresponding relationship between aperture and melting point can be obtained as follows:

$$D = \frac{k}{\Delta T_m} \approx \frac{39.6}{\Delta T_m}(\text{nm}). \quad (3)$$

According to Kekkonen et al. [27], it is estimated that there exists a nonfreezing layer of water with a thickness of 0.3 nm (one water molecule thickness); the nonfreezing layer of water may be a two-dimensional ice structure. The echo time in the CPMG sequence was 0.1 ms; the relaxation time of the nonfreezing layer was too short (like solid, a few microseconds) and was not detectable in the experiments. If the pores within the cell wall are assumed to be cylindrical, it is necessary to increase two layers of water molecule thickness (0.6 nm) on the basis of the Gibbs-Thomson equation. The relationship between the temperature drop of the freezing point and pore diameter is shown in Table 2.

Table 3: Salt solutions used in the sorption experiment and registered relative humidity at 25°C.

| Salt | RH (%) |
|---|---|
| Potassium nitrate ($KNO_3$) | 93.6 |
| Potassium chloride (KCl) | 84.3 |
| Sodium chloride (NaCl) | 75.3 |
| Sodium bromide (NaBr) | 57.6 |
| Potassium carbonate ($K_2CO_3$) | 43.2 |
| Potassium acetate ($CH_3COOK$) | 22.5 |
| Lithium chloride (LiCl) | 11.3 |

*2.5. Determination of the Moisture Content, FSP, and Pore Size Distribution.* The moisture content (MC) of the samples was determined by the weight difference between the saturated and dried samples (103 ± 2°C, 24 h), and it was calculated by equation (4). Here, $m_w$ and $m_d$ are the masses of the sample before and after drying, respectively.

$$\mathrm{MC} = \frac{m_w - m_d}{m_d} \bullet 100\%. \quad (4)$$

The FSP of the cell wall is obtained from the following equation:

$$\mathrm{FSP} = \mathrm{MC} \bullet \frac{S_c}{S_n}, \quad (5)$$

where MC is the moisture content, $S_c$ represents the NMR signal amplitude of the sample at the critical temperature point in the low temperature NMR experiment, and $S_n$ represents the NMR signal at room temperature. In order to eliminate the influence of temperature during experiments, the signal amplitudes measured at the critical temperature were multiplied by factor $T/T_0$, where $T$ is the actual temperature and $T_0$ is the reference temperature [15]. In this paper, the 0°C (273 K) was selected as the reference temperature. The critical temperature can be determined by the variation of the sample NMR signal amplitude with the experiment temperature. There were two kinds of typical scales for wood pore structure: lumens are micron scale and micropores within the cell wall are nanoscale. The melting point of moisture in the cell wall and lumen is significantly different. Therefore, the critical temperature can be determined by the change of the NMR signal amplitude with temperature ($dS/dT$). At the critical temperature, the free water in the lumens is frozen and bound water in the cell wall is liquid.

The pore size distribution within the cell wall is determined by the NMR signal amplitude of the sample corresponding to the pore size with a certain melting temperature given by the Gibbs-Thomson equation according to Table 2. The diameter distribution proportion within a certain range could be determined by

$$\mathrm{PD} = \frac{S_a - S_b}{\mathrm{FSP}}, \quad (6)$$

where $S_a$ and $S_b$ are the NMR signal amplitude of the sample at temperatures a and b, respectively, and the temperature corresponds to the pore diameter.

*2.6. Adsorption Isotherm Test.* The test samples were kept above saturated solutions of various salts in containers stored in an incubator set at 25°C (±0.2°C). Seven salts were chosen, and these are listed in Table 3 [36]. The samples of dimension 20 mm × 20 mm × 5 mm (radial × tangential × longitudinal) were cut from discs. Due to the longer growth time, the heartwood and sapwood of two kinds of Chinese fir (F24×Na 1-1, Kaihua 13) could be clearly distinguished. Therefore, the heartwood and sapwood of the two types of Chinese fir were separated during sample preparation. The difference between the heartwood and sapwood of poplar and another Chinese fir (Yang 020) is not obvious, so they were not distinguished during sample preparation. After the adsorption isotherm test, the samples were dried at 103 ± 2°C for 24 h, and the equilibrium moisture content at different values of relative humidity was calculated.

The three-parameter GAB sorption equation (7) is used to interpret the equilibrium moisture content.

$$V = V_m \frac{C \times K \times \mathrm{RH}}{(1 - K \times \mathrm{RH})(1 - K \times \mathrm{RH} + C \times K \times \mathrm{RH})}, \quad (7)$$

where $V$ is the volume of water vapor adsorbed per unit mass of absolute dry wood after a certain temperature and humidity environment is balanced ($cm^3 \cdot g^{-1}$), and $V_m$ is the adsorption water content of monolayer molecules ($cm^3 \cdot g^{-1}$), $C$ is the constant related to the difference between the free enthalpy (compared to the standard chemical potential) between the adsorption of water by a single layer of molecules and the adsorption of water by the multilayer molecules formed on it, and $K$ is the free enthalpy of adsorption of water and pure water by the multilayer molecules with the constant related to the difference. RH is the relative humidity of the isotherm adsorption process [36]. The fitting of the adsorption isotherm was done using the OriginPro 8.0 software by least-square regression.

## 3. Results and Discussion

*3.1. NMR Signal Amplitude Change with Temperature and the Critical Temperature to Determine FSP.* The NMR signal amplitude and its differential curve of the sample under different temperatures are presented in Figure 1. The NMR signal amplitude of the samples increase continuously with the increase of the experimental temperature. As mentioned earlier, the $T_2$ relaxation time of the macromolecule of the cell wall and the frozen water (ice) is approximately 10 $\mu$s and 6 $\mu$s, respectively [15]. They were not detectable in the $T_2$ measurements when the echo time in the sequence was 0.1 ms, and the NMR signals arise exclusively from the unfrozen moisture in the samples. As the temperature of the samples continues to increase, the frozen moisture in the samples gradually melt, and the amount of the detectable moisture also continues to increase. The NMR signal amplitude of the samples increases sharply near 0°C and then

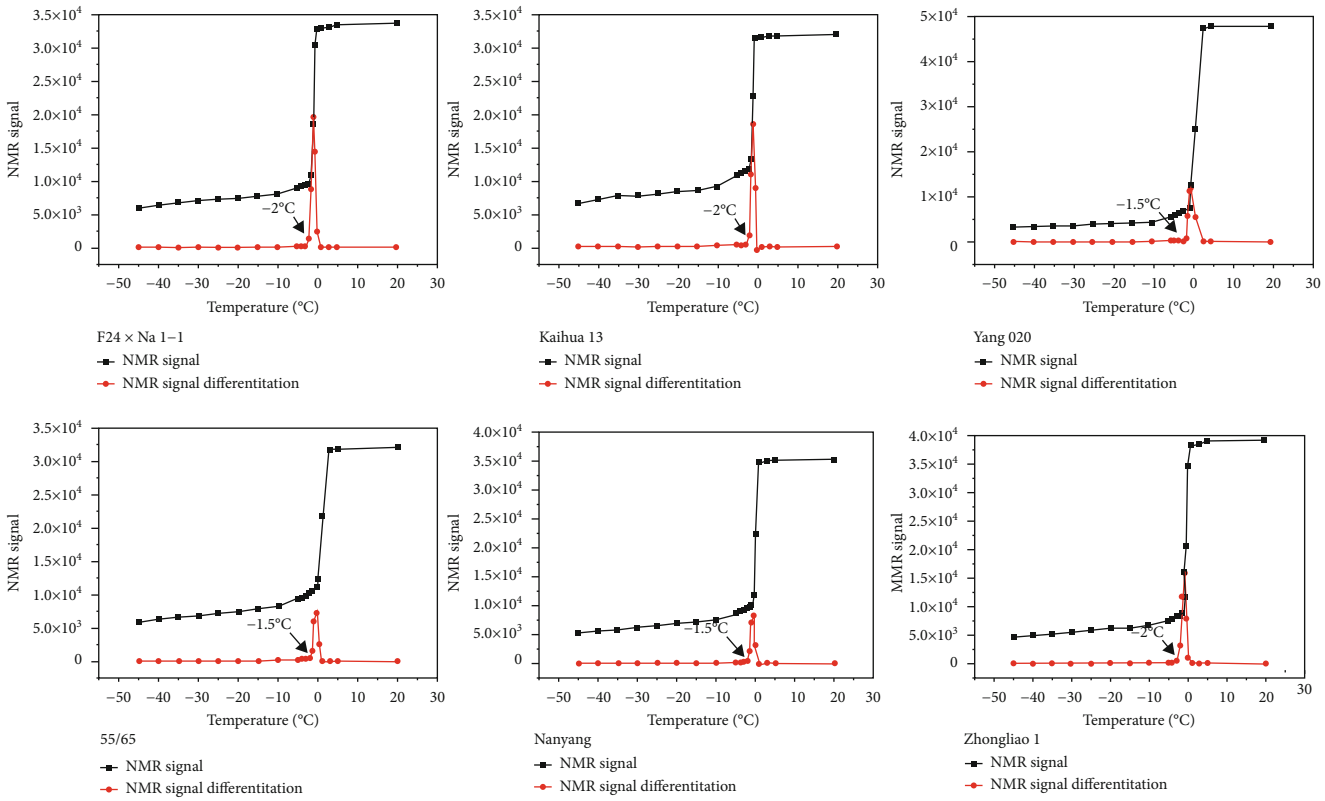


Figure 1: Changes of NMR signals at different temperatures.

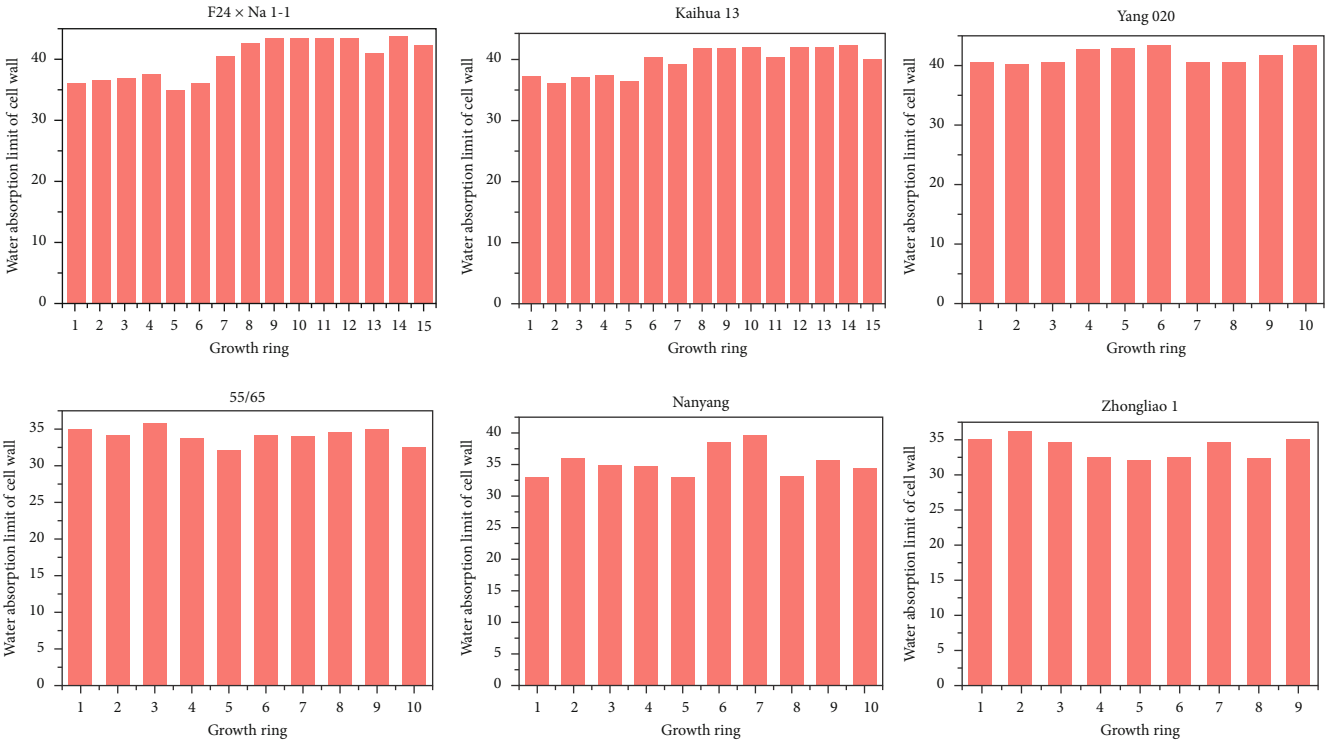


Figure 2: Water absorption limit of the cell wall in different growth rings.

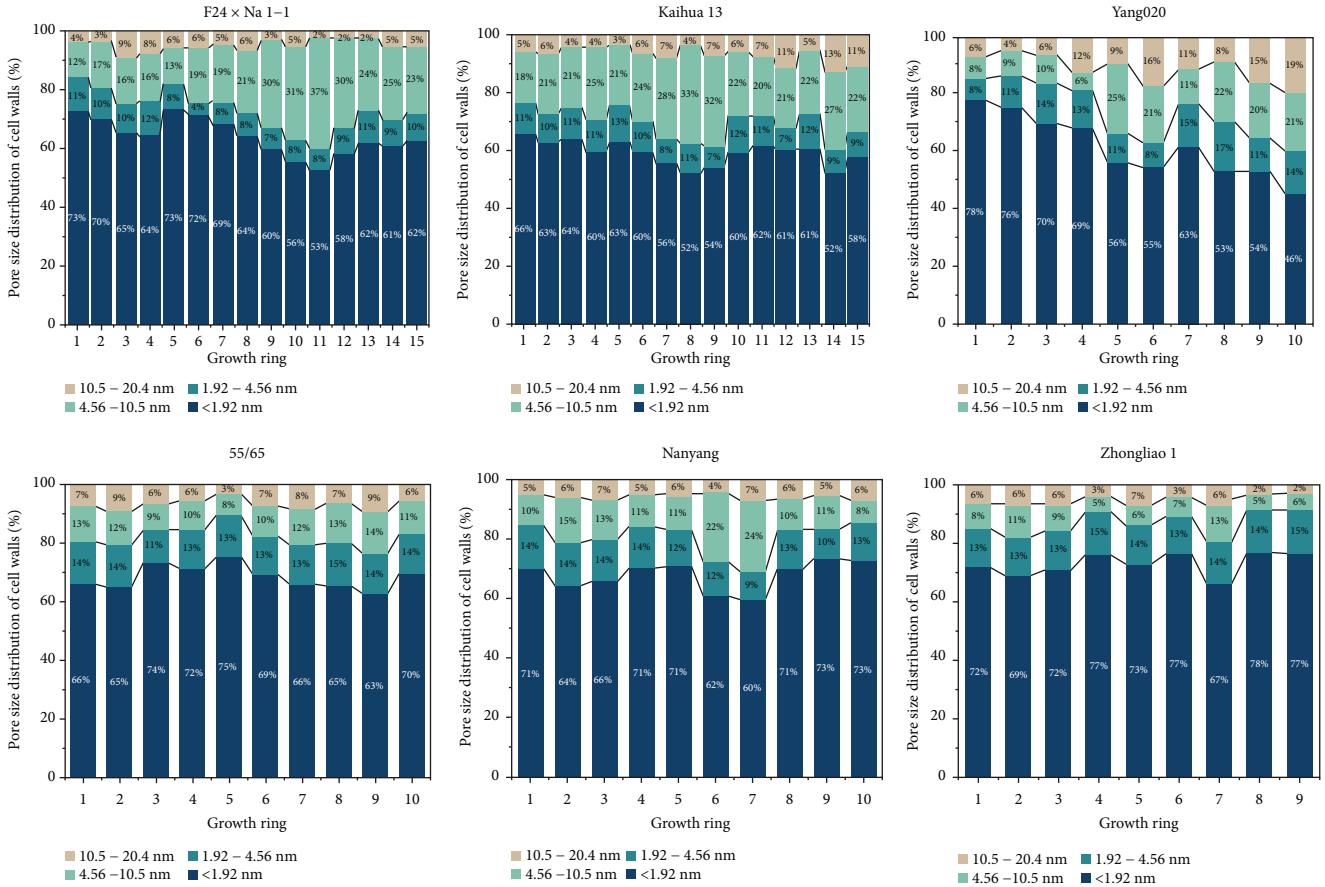


Figure 3: Pore size distribution in different growth rings.

remains unchanged, which should be attributed to the melting of the frozen free water in the lumens.

According to the Gibbs-Thomson equation, the melting point depression is inversely proportional to the diameter of the pore, the diameters of the lumens are micron scale, and the micropores in the cell wall are nanoscale. There is a critical temperature that the free water in the lumens is frozen and the bound water is liquid. The critical temperature can be determined from the differentiation of the NMR signal amplitude of the sample (solid line with red dots). There is no significant change in the differential of the NMR signal amplitude with temperature when the temperature is low. However, when the experiment temperature is close to the -2°C–-1.5°C, the differential of the NMR signal amplitude changes significantly. In this study, -2°C was used as the critical temperature, at which the free water in lumens is frozen and the bound water in the cell wall is liquid.

*3.2. The FSP of Chinese Fir and Poplar Clones.* The FSP of Chinese fir and poplar of different growth rings are presented in Figure 2. The average FSP of three Chinese fir clones was 40.13% (F24×Na 1-1), 40.25% (Kaihua 13), and 41.72% (Yang 020); the maximum FSP was 43.81% (F24×Na 1-1), 42.88% (Kaihua 13), and 43.63% (Yang 020). Although there was no obvious difference in the FSP between species, there were certain differences in the FSP between different growth rings of the same species. The FSP of F24×Na 1-1 and Kaihua 13 showed a trend of increasing from heartwood to sapwood. The 7th growth ring was the boundary of the heartwood and sapwood. The heartwood FSP of F24×Na 1-1 and Kaihua 13 was 36.93% and 38.19%, respectively, and the sapwood FSP of F24×Na 1-1 and Kaihua 13 was 42.92% and 42.06%, respectively. The difference in the FSP of the heartwood and sapwood can be attributed to the difference of the content of extractives. During the formation of heartwood, living cells gradually died, and sediment such as tannin, pigment, and calcium carbonate appeared in the cell cavity. The water transport system was blocked, the density increased, and the permeability decreased. Therefore, the deposition of extractive occupied some micropores in the cell wall; the decrease in permeability is also strong evidence of the decrease in porosity [37]. The Yang 020 contained 10 growth rings, and only two growth rings belonged to sapwood. The growth time of the tree was short, and the corresponding deposition and conversion of extractives was short, so the difference in the FSP between heartwood and sapwood was not significant.

The difference between poplar's heartwood and sapwood is not significant, and the FSP between different growth rings and species is also not significant. The average FSP of the three poplar clones was 34.15% (55/65), 35.26% (Nanyang), and 33.78% (Zhongliao 1), which was obviously lower than that of Chinese fir. The difference in the FSP between poplar and Chinese fir can be attributed to the difference of basic

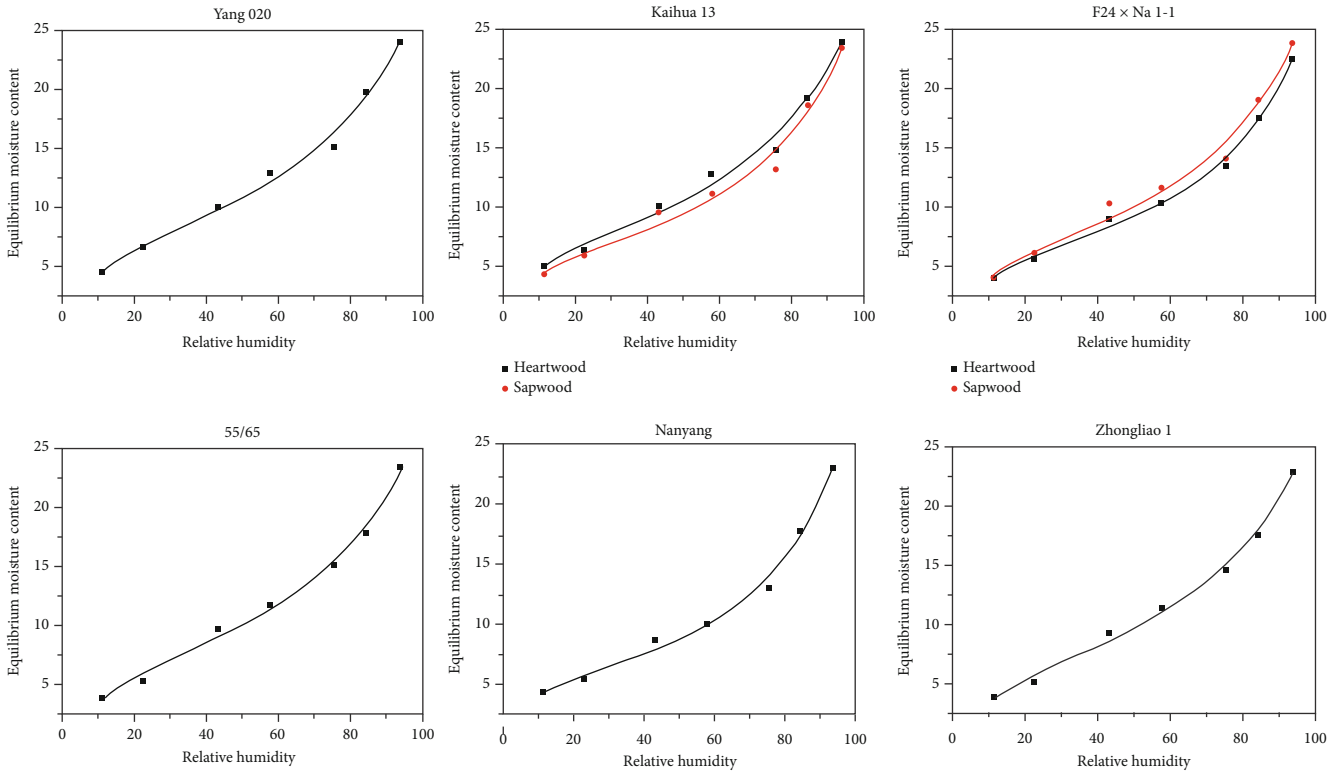


Figure 4: Adsorption isotherm of six species of tree sample.

Table 4: Fitted constants calculated for the GAB equation adsorption isotherms.

| Species | $V_m$ ($cm^3 \cdot g^{-1}$) | $C$ | $K$ | $R^2$ |
|---|---|---|---|---|
| F24×Na 1-1 (heartwood) | 0.06031 | 18.5284 | 0.7855 | 0.99 |
| F24×Na 1-1 (sapwood) | 0.06949 | 14.3781 | 0.762 | 0.98 |
| Kaihua 13 (heartwood) | 0.0726 | 17.8973 | 0.7486 | 0.98 |
| Kaihua 13 (sapwood) | 0.06111 | 20.7627 | 0.7938 | 0.98 |
| Yang 020 | 0.07733 | 13.5903 | 0.7344 | 0.99 |
| 55/65 | 0.07306 | 10.2382 | 0.7428 | 0.99 |
| Nanyang | 0.05527 | 22.2837 | 0.8162 | 0.99 |
| Zhongliao 1 | 0.0703 | 10.1092 | 0.7473 | 0.99 |

density. The basic density of Chinese fir and poplar was 0.3~0.35 g/cm$^3$ and 0.39~0.43 g/cm$^3$, respectively. It is suggested that with decreasing basic density, the thickness of cell wall decreases, and the cell wall displays less resistance to swelling. The bound water content that corresponds to the FSP represents a balance between the swelling of the cell wall and resistance to the mechanical rigidity [38].

The FSP of Chinese fir and poplar was both higher than 30%, which is the typical value measured by extrapolation methods. The extrapolation methods are based upon conditioning wood at different values of relative humidity and measuring the moisture content of wood. Then, the FSP will be determined by extrapolating the measured sorption isotherm to 100% relative humidity [17]. However, the FSP determined by extrapolation may underestimate the saturated content of bound water. Methods including solute exclusion, porous plate, DSC, and NMR, which are supposed to measure the bound water content of the swollen cell wall, may result in FSP values above 40% [15]. It was found that the specimens that were conditioned at 100% relative humidity would further swell when soaked in water; therefore, it is reasonable to believe that the limitation of bound water would be underestimated by the extrapolation method [17]. In addition to the definition of the FSP, "the moisture content when the cell wall is saturated and the lumens do not contain free water," there are other definitions, such as the FSP proposed by Stone and Scallan [39]: "the amount of water contained within the water saturated cell wall." In the present study, the latter definition of FSP will be followed, and the FSP of Chinese fir and poplar were close to the values detected by the solute exclusion [40], porous plate [41], DSC [35], and NMR methods [15].

*3.3. Pore Size Distribution of Cell Walls.* The pore size distributions in the cell wall of Chinese fir and poplar clones are presented in Figure 3. For the Chinese fir, the proportion of pores with the diameter smaller than 1.92 nm approximately ranged from 50% to 80%, the proportion of pores with the diameter between 1.92 nm and 4.56 nm approximately ranged from 5% to 15%, the proportion of pores with the diameter between 4.56 nm and 10.5 nm approximately ranged from 10% to 30%, and the proportion of pores with the diameter greater than 10 nm was less than 20%. For the poplar, the proportion of pores with the diameter smaller

Table 5: FSP was measured by different methods.

| Species | $V_{\text{monolayer}}$ | $V_{\text{multilayer}}$ | FSP* | FSP | FSP – FSP* | $\frac{\text{FSP} - \text{FSP}^*}{\text{FSP}}$ |
|---|---|---|---|---|---|---|
| F24×Na 1-1 (heartwood) | 6.03% | 21.67% | 27.70% | 37.65% | 9.95% | 26.43% |
| F24×Na 1-1 (sapwood) | 6.94% | 21.64% | 28.58% | 42.92% | 14.37% | 33.48% |
| Kaihua 13 (heartwood) | 7.26% | 21.09% | 28.35% | 38.69% | 10.34% | 26.73% |
| Kaihua 13 (sapwood) | 6.11% | 23.16% | 29.27% | 42.04% | 12.77% | 30.38% |
| Yang 020 | 7.73% | 20.63% | 28.36% | 41.72% | 13.36% | 32.02% |
| 55/65 | 7.31% | 22.46% | 29.77% | 34.15% | 4.38% | 12.83% |
| Nanyang | 5.53% | 21.95% | 27.48% | 35.26% | 7.78% | 22.06% |
| Zhongliao 1 | 7.03% | 20.45% | 27.48% | 33.78% | 6.30% | 18.65% |

than 1.92 nm approximately ranged from 60% to 75%, the proportion of pores with the diameter between 1.92 nm and 4.56 nm approximately ranged from 10% to 15%, the proportion of pores with the diameter between 4.56 nm and 10.5 nm approximately ranged from 5% to 20%, and the proportion of pores with the diameter greater than 10 nm was less than 10%. The results indicated that the majority of the pores within the cell wall were relatively minute and the pore size distributions were not homogeneous; this corresponded to the results by the solute exclusion method [38] and NMR cryoporometry [18]. The pore size distributions are different depending on the species; this could be attributed to the differences of the microstructure between different species, such as the differences in the diameters of the microfibrils between species; this may influence the size of minipores existing between the microfibrils [42].

Compared with other species, the proportion of pores with the diameter smaller than 1.92 nm of F24×Na 1-1 and Kaihua 13 showed a decreasing trend from pith to sapwood. On the contrary, the proportion of pores with the diameter greater than 4.56 nm showed an increasing trend from pith to sapwood. It was indicated that the pore structure of the cell wall near the pith was relatively "dense," while the pore structure of the cell wall near the sapwood was relatively "loose." The difference in the pore size distribution from pith to sapwood of poplar was not significant, and this could also be attributed to the difference in the heartwood and sapwood. As the extractives deposited and diffused in wood tissue, the sapwood transformed into heartwood. It was possible that a part of the relatively "loose" cell wall was deposited with extractives, which turned into a "dense" cell wall. The closer to the pith, the longer the deposition and transformation time will be. The pore size distribution of the cell wall is helpful for the selection of wood, such as the particle size of the functional nanoparticles and the molecular weight of the resins.

Considering that the volume of the liquid water will expand when it freezes into ice, there is bound to be some error. However, due to the elasticity of the wood, when the ice melts, the gap may recover to some extent, so there will still be some unknown errors. Due to the limitation of the experimental method, this is inevitable, but the error is controlled within a small range, and the study of this method is still meaningful.

*3.4. Adsorption Isotherm and the Content of Different Types of Bound Water.* The adsorption isotherms of Chinese fir and poplar clones were presented in Figure 4, and the GAB constants were determined by least-square regression of sorption data in the range 11.3% to 93.6%. The values of GAB constants obtained from the regression of the EMC at various values of relative humidity are listed in Table 4. The correlation factor ($R^2$) was greater than 0.98, indicating that the GAB equation was a good description of the relationship between the relative humidity and EMC of different species. All samples exhibited the Type II sigmoidal adsorption isotherms according to the IUPAC 1985 classification (Donohue and Aranovich, 1988). The values of adsorption regression coefficients ($V_m$, $C$, $K$) were similar to some researchers' results [36, 43].

As mentioned earlier, the FSP will be determined by extrapolating the measured sorption isotherm to 100% relative humidity; the fitted constants in Table 4 were used, and the FSP* determined by the extrapolation method can be calculated. The advantage of the GAB model is that this model is particularly appropriate when the relative humidity is greater than 90%. However, when the relative humidity of the environment is high, for example, higher than 98%, capillary condensation may occur in wood according to the Kelvin equation [38]. Nevertheless, it was still hypothesized that the GAB model is correct and that only the water vapor adsorption occurs in the wood when the relative humidity is 100%. The monolayer molecule water content ($V_{\text{monolayer}}$), multilayer molecular water content ($V_{\text{multilayer}}$), and FSP determined from NMR are listed in Table 5. The value of FSP* determined by the extrapolation method ranged from 27.48% to 29.77%, which was close to 30%. The difference between FSP (NMR method) and FSP* (extrapolation method) was approximately 5% to 14%. If the moisture in the cell wall is calculated as a percentage, this part of the moisture accounts for about 13% to 30% of the total bound water in the cell wall. Its proportion is roughly the same as the proportion of minipores within the cell wall with the diameter greater than about 5 nm. The authors considered that this part of moisture only exists in the relative "large pores" which appear when the wood contains free water to swell the cell wall. The bound water can be divided into the monolayer water, multilayer water, and "free bound water" [15]; the moisture of the difference between the NMR method and the extrapolation method in this work

may correspond to the "free bound water." Hence, the combination of NMR and the isothermal adsorption method may be more beneficial to the analysis of the moisture in wood. However, additional experiment methods, for example, DSC, should be performed to confirm this interpretation.

## 4. Conclusions

In this study, six species of fast-growing forest wood, which are widely cultivated and planted in China, were analyzed by NMR technology. The FSP and pore size distributions within were determined by NMR cryoporometry. The average FSP of three Chinese fir clones was approximately higher than 40%, and the average FSP of the three poplar clones was approximately 35%. The differences in FSP between different species and growth rings mainly depended on the basic density and extractives of wood samples. The majority of the pores within the cell wall were relatively minute, and the pore size distributions were not homogeneous. The proportion of pores with the diameter smaller than 1.92 nm approximately was higher than 50%, and the proportion of pores with the diameter greater than 10 nm was less than 20%. The difference in pore size distributions between different species and different growth rings can be attributed to the differences of the microstructure and the extractives between different species. The water vapor sorption experiments were performed, and the adsorption isotherms of the samples were fitted through the GAB equation. Combined with the actual value of the FSP determined by the NMR method, the content of the monolayer molecule water, multilayer molecular water, and "free bound water" was analyzed. This work will be helpful to the study of the wood moisture status and provide reference data for wood modification.

## Data Availability

The data used to support the findings of this study are available from the corresponding author upon request.

## Conflicts of Interest

The authors declare that they have no conflicts of interest.

## Acknowledgments

This research was sponsored by the National Natural Science Foundation of China (31971591) and National Key Research and Development Program of China (2017YFD0600202).

## References

[1] A. Lozhechnikova, H. Bellanger, B. Michen, I. Burgert, and M. Österberg, "Surfactant-free carnauba wax dispersion and its use for layer-by-layer assembled protective surface coatings on wood," *Applied Surface Science*, vol. 396, pp. 1273–1281, 2017.

[2] Y. Li and J. Li, "Fabrication of reversible thermoresponsive thin films on wood surfaces with hydrophobic performance," *Progress in Organic Coating*, vol. 119, pp. 15–22, 2018.

[3] China National Forestry and Grassland Administration, *China Forestry and Grassland Statistical Yearbook*, China Forestry Publishing House, Beijing, China, 2019.

[4] H. Chen, "Phosphatase activity and P fractions in soils of an 18-year-old Chinese fir (*Cunninghamia lanceolata*) plantation," *Forest Ecology and Management*, vol. 178, no. 3, pp. 301–310, 2003.

[5] Y. Zhang, S. F. Yuan, K. H. Wang, and Q. Li, "Study on the effects of microwave pretreatment on the fire retardant permeability of fast-growing wood," *Applied Mechanics and Materials*, vol. 423-426, pp. 1334–1338, 2013.

[6] Ö. Gezici-Koç, S. J. F. Erich, H. P. Huinink, L. G. J. van der Ven, and O. C. G. Adan, "Bound and free water distribution in wood during water uptake and drying as measured by 1D magnetic resonance imaging," *Cellulose*, vol. 24, no. 2, pp. 535–553, 2017.

[7] K. Xu, S. Yuan, Y. Gao et al., "Characterization of moisture states and transport in MUF resin-impregnated poplar wood using low field nuclear magnetic resonance," *Drying Technology*, vol. 39, pp. 791–802, 2021.

[8] E. H. Wong, "Characterizing the kinetics of free and bound water using a non-isothermal sorption technique," *Drying Technology*, vol. 35, no. 1, pp. 46–54, 2017.

[9] E. Perem, "Determination of the fiber saturation point of wood by centrifuging," *Forest Products Journal*, vol. 4, no. 2, pp. 77–81, 1954.

[10] P. A. Ahlgren, J. R. Wood, and D. Goring, "The fiber saturation point of various morphological subdivisions of Douglas-fir and aspen wood," *Wood Science and Technology*, vol. 6, no. 2, pp. 81–84, 1972.

[11] W. J. Cousins, "Elastic modulus of lignin as related to moisture content," *Wood Science and Technology*, vol. 10, no. 1, pp. 9–17, 1976.

[12] W. Cousins, "Young's modulus of hemicellulose as related to moisture content," *Wood Science and Technology*, vol. 12, no. 3, pp. 161–167, 1978.

[13] L. A. Simpson and A. Barton, "Determination of the fibre saturation point in whole wood using differential scanning calorimetry," *Wood Science and Technology*, vol. 25, no. 4, pp. 301–308, 1991.

[14] I. D. Hartley, F. A. Kamke, and H. Peemoeller, "Absolute moisture content determination of aspen wood below the fiber saturation point using pulsed NMR," *Holzforschung*, vol. 48, no. 6, pp. 474–479, 1994.

[15] V. V. Telkki, M. Yliniemi, and J. Jokisaari, "Moisture in softwoods: fiber saturation point, hydroxyl site content, and the amount of micropores as determined from NMR relaxation time distributions," *Holzforschung*, vol. 67, 2013.

[16] M. Zauer, J. Kretzschmar, L. Großmann, A. Pfriem, and A. Wagenführ, "Analysis of the pore-size distribution and fiber saturation point of native and thermally modified wood using differential scanning calorimetry," *Wood Science and Technology*, vol. 48, no. 1, pp. 177–193, 2014.

[17] M. Babiak and J. Kúdela, "A contribution to the definition of the fiber saturation point," *Wood Science and Technology*, vol. 29, no. 3, pp. 217–226, 1995.

[18] X. Gao, S. Zhuang, J. Jin, and P. Cao, "Bound water content and pore size distribution in swollen cell walls determined by

NMR technology," *BioResources*, vol. 10, no. 4, pp. 8208–8224, 2015.

[19] T. Furuno, Y. Imamura, and H. Kajita, "The modification of wood by treatment with low molecular weight phenol-formaldehyde resin: a properties enhancement with neutralized phenolic-resin and resin penetration into wood cell walls," *Wood Science and Technology*, vol. 37, no. 5, pp. 349–361, 2004.

[20] S. Vitas, J. S. Segmehl, I. Burgert, and E. Cabane, "Porosity and pore size distribution of native and delignified beech wood determined by mercury intrusion porosimetry," *Materials*, vol. 12, no. 3, p. 416, 2019.

[21] P. Grönquist, M. Frey, T. Keplinger, and I. Burgert, "Mesoporosity of delignified wood investigated by water vapor sorption," *ACS Omega*, vol. 4, no. 7, pp. 12425–12431, 2019.

[22] O. Galmiz, R. Talviste, R. Panáček, and D. Kováčik, "Cold atmospheric pressure plasma facilitated nano-structuring of thermally modified wood," *Wood Science and Technology*, vol. 53, no. 6, pp. 1339–1352, 2019.

[23] S. J. Hanley and D. G. Gray, "Atomic force microscope images of black spruce wood sections and pulp fibres," *Holzforschung*, vol. 48, no. 1, pp. 29–34, 1994.

[24] H. Matsunaga, M. Kiguchi, and P. D. Evans, "Microdistribution of copper-carbonate and iron oxide nanoparticles in treated wood," *Journal of Nanoparticle Research*, vol. 11, no. 5, pp. 1087–1098, 2009.

[25] H. Westphal, I. Surholt, C. Kiesl, H. F. Thern, and T. Kruspe, "NMR measurements in carbonate rocks: problems and an approach to a solution," *Pure and Applied Geophysics*, vol. 162, no. 3, pp. 549–570, 2005.

[26] H. H. Tian, C. F. Wei, H. Z. Wei, R. T. Yan, and P. Chen, "An NMR-based analysis of soil–water characteristics," *Applied Magnetic Resonance*, vol. 45, no. 1, pp. 49–61, 2014.

[27] P. M. Kekkonen, A. Ylisassi, and V. V. Telkki, "Absorption of water in thermally modified pine wood as studied by nuclear magnetic resonance," *The Journal of Physical Chemistry C*, vol. 118, no. 4, pp. 2146–2153, 2014.

[28] M. A. Javed, P. M. Kekkonen, S. Ahola, and V. V. Telkki, "Magnetic resonance imaging study of water absorption in thermally modified pine wood," *Holzforschung*, vol. 69, no. 7, pp. 899–907, 2015.

[29] N. Labbé, B. De Jéso, J.-C. Lartigue, G. Daudé, M. Pétraud, and M. Ratier, "Time-domain 1H NMR characterization of the liquid phase in greenwood," *Holzforschung*, vol. 60, no. 3, pp. 265–270, 2006.

[30] M. Merela, P. Oven, I. Serša, and U. Mikac, "A single point NMR method for an instantaneous determination of the moisture content of wood," *Holzforschung*, vol. 63, no. 3, pp. 348–351, 2009.

[31] C. Casieri, L. Senni, M. Romagnoli, U. Santamaria, and F. De Luca, "Determination of moisture fraction in wood by mobile NMR device," *Journal of Magnetic Resonance*, vol. 171, no. 2, pp. 364–372, 2004.

[32] H. Penvern, M. Zhou, B. Maillet et al., "How bound water regulates wood drying," *Physical Review Applied*, vol. 14, no. 5, 2020.

[33] M. Bonnet, D. Courtier-Murias, P. Faure, S. Rodts, and S. Care, "NMR determination of sorption isotherms in earlywood and latewood of Douglas fir. Identification of bound water components related to their local environment," *Holzforschung*, vol. 71, no. 6, pp. 481–490, 2017.

[34] J. Cox, P. J. Mcdonald, and B. A. Gardiner, "A study of water exchange in wood by means of 2D NMR relaxation correlation and exchange," *Holzforschung*, vol. 64, no. 2, pp. 259–266, 2010.

[35] S. Park, R. Venditti, H. Jameel, and J. Pawlak, "Changes in pore size distribution during the drying of cellulose fibers as measured by differential scanning calorimetry," *Carbohydrate Polymers*, vol. 66, no. 1, pp. 97–103, 2006.

[36] W. Olek, J. Majka, and Ł. Czajkowski, "Sorption isotherms of thermally modified wood," *Holzforschung*, vol. 67, no. 2, pp. 183–191, 2013.

[37] F. F. P. Kollmann, E. W. Kuenzi, and A. J. Stamm, "Principles of wood science and technology," in *I Solid Wood*, Springer, 1968.

[38] J. Walker, *Primary Wood Processing: Principles and Practice*, Springer, University of Canterbury, Christchurch, New Zealand, 2006.

[39] J. E. Stone and A. M. Scallan, "Effect of component removal upon the porous structure of the cell wall of wood," *Journal of Polymer Science Part C: Polymer Symposia*, vol. 11, no. 1, pp. 13–25, 1965.

[40] C. A. S. Hill, "Wood modification (chemical, thermal and other processes)," in *The Use of Timber in the Twenty-first Century*, pp. 1–18, Wiley, 2006.

[41] A. Cloutier and Y. Fortin, "Moisture content—water potential relationship of wood from saturated to dry conditions," *Wood Science and Technology*, vol. 25, no. 4, pp. 263–280, 1991.

[42] L. Donaldson, "Cellulose microfibril aggregates and their size variation with cell wall type," *Wood Science and Technology*, vol. 41, no. 5, pp. 443–460, 2007.

[43] Ł. Bratasz, A. KozłOwska, and R. KozłOwski, "Analysis of water adsorption by wood using the Guggenheim-Anderson-de Boer equation," *European Journal of Wood and Wood Products*, vol. 70, no. 4, pp. 445–451, 2012.